Structural, magnetic, electronic, and elastic properties of face-centered cubic PuH_x ($x = 2, 3$) : GGA (LSDA) + U + SO*

Guo Yong(郭 咏)[a], Ai Juan-Juan(艾娟娟)[a], Gao Tao(高 涛)[a]†, and Ao Bing-Yun(敖冰云)[b]‡

[a] *Institute of Atomic and Molecular Physics, Sichuan University, Chengdu* 610065, *China*

[b] *Science and Technology on Surface Physics and Chemistry Laboratory, P.O. Box* 718-35, *Mianyang* 621907, *China*

(Received 30 October A 2012; revised manuscript received 25 December 2012)

We perform first-principles calculations to investigate the structural, magnetic, electronic, and mechanical properties of face-centered cubic (fcc) PuH_2 and fcc PuH_3 using the full potential linearized augmented plane wave method (FP-LAPW) with the generalized gradient approximation (GGA) and the local spin density approximation (LSDA) taking account of both relativistic and strong correlation effects. The optimized lattice constant $a_0 = 5.371$ Å for fcc PuH_2 and $a_0 = 5.343$ Å for fcc PuH_3 calculated in the GGA + sp (spin polarization) + U (Hubbard parameter) + SO (spin–orbit coupling) scheme are in good agreement with the experimental data. The ground state of fcc PuH_3 is found to be slightly ferromagnetic. Our results indicate that fcc PuH_2 is a metal while fcc PuH_3 is a semiconductor with a band gap about 0.35 eV. We note that the SO and the strong correlation between localized Pu 5f electrons are responsible for the band gap of fcc PuH_3. The bonds for PuH_2 have mainly covalent character while there are covalent bonds in addition to apparent ionicity bonds for PuH_3. We also predict the elastic constants of fcc PuH_2 and fcc PuH_3, which were not observed in the previous experiments.

Keywords: plutonium hydride, density-functional theory, magnetic and elastic properties, metal–insulator transition

PACS: 71.27.+a, 71.30.+h, 71.70.Ej **DOI:** 10.1088/1674-1056/22/5/057103

1. Introduction

Numerous interesting physical properties, not only of the nuclearity but also of the electronicity, were brought about among actinide elements, resulting from the 5f states of the actinide elements.[1] It has become a central topic of physics, as well as an attractive field for understanding the 5f states of actinides (Ac).[2–6] In the series, Pu is located at a special site where the transition of 5f electrons from itinerancy to localization occurs.[2,7] So Pu becomes the most complex element with many anomalous properties.[1]

Increasing experimental and theoretical efforts have been made toward profoundly understanding the 5f electronic nature of Pu metals and its compounds. Nevertheless, experimental observations are scarce because of its toxic and radioactive nature.[1] The density-functional theory (DFT) is a ground-state theory, which is good at calculating the electronic structure of materials as well as the bonding properties, such as crystal structures, bulk moduli, elastic constants, and magnetism.[1,8] Hence, more and more first-principles techniques from the traditional DFT to DFT+U and dynamical mean field theory (DMFT)[9] have been performed to explore the electronic structure of Pu materials during the last three decades. Moore *et al.* reviewed that there are still many unanswered questions about the electronic structure, magnetism, and character of bonding.[1] Pu oxides have been studied theoretically to answer those questions. Sun *et al.* used the DFT+U to study the structural, electronic, and thermodynamic properties of PuO_2 and Pu_2O_3.[10] Liu *et al.* obtained the electronic, structural properties and elastic constants of δ-Pu and PuO by using the LSDA/GGA + U method.[11] Wang *et al.* performed a calculation on PuO_2 within a local density approximation (LDA) + U scheme to investigate its structural, mechanical, magnetic, and intrinsic bonding properties.[12] In particular, Ao *et al.* first predicted the metal–insulator transition in the Pu–H system theoretically and also researched the lattice contraction of face-centered cubic (fcc) Pu hydrides within the LDA+U frame.[2–4] However, the theoretical study of magnetism and mechanical properties of Pu hydrides is still lacking. In addition, the spin–orbit coupling (SO) of the 5f electrons has not been included in the previous works, while it plays a pivotal role for Pu 5f electrons.[13,14] Hence, we consider not only U but also the SO effects on Pu 5f states. Our calculations are based on the experimental results that fcc PuH_2 is ferromagnetic,[15,16] while the magnetism of fcc PuH_3 is uncertain. We investigate the magnetic stability of fcc PuH_3. The mechanical properties are calculated first.

The present paper is organized as follow. In Section 2, we give the details of our calculation. The results and discussion are presented in Section 3. Finally, the conclusions are summarized in Section 4.

*Project supported by the National Natural Science Foundation of China (Grant No. 20971114).

†Corresponding author. E-mail: gaotao@scu.edu.cn

‡Corresponding author. E-mail: aobingyun24@yahoo.com.cn

© 2013 Chinese Physical Society and IOP Publishing Ltd

2. Computational method

The calculations are carried out using the full potential linearized augmented plane wave method (FP-LAPW) method implemented in the WIEN2K code.[17,18] The exchange–correlation potential is computed with the generalized gradient approximation (GGA) and the local spin density approximation (LSDA). The unit cell is divided into non-overlapping atomic spheres whose centers are at atomic positions, and interstitial region. Inside the muffin-tin region, the potential is a product of radial function and spherical harmonics. For the interstitial region, i.e., outside the muffin-tin sphere, the potential is expanded in plane waves. The muffin-tin radii R_{MT} are chosen so that the spheres are not overlapped. The muffin-tin radii R_{MT} of Pu and H atoms are 2.3 a.u. and 0.9 a.u., respectively. The charge convergence is set to 0.0001, and the total energy convergence is set to 0.0001 Ry for all the iterations. The separation energy is -6.0 Ry in the calculation of the exchange–correlation energy. The cutoff parameter $R_{MT}K_{MAX}$ is set to 3 for both PuH_2 and PuH_3. Here K_{MAX} is the maximum modulus for the reciprocal lattice vector. K-points are taken as 5000 in GGA (+ sp/ + sp+ U/ + sp + U + SO) and 15000 in LSDA (+ sp/ + sp + U/+ sp + U + SO) for PuH_2. The $1\times1\times1$ supercell of fcc PuH_3 is constructed and used in all our calculations because of the calculation of antiferromagnetism and 100 K-points is used for PuH_3 to save computing resources and time. The value of U is optimized to be 4.00 eV for PuH_2 and PuH_3.[3] Moreover, local orbitals have been added for all atoms and valence states. Furthermore, the spin–orbit coupling is included in the calculations based on the second variational approach.[19]

The crystal structures are shown in Figs. 1(a) and 1(b). The structure of PuH_2 is equivalent to that of CaF_2, whose space group is $Fm3m$ as seen in Fig. 1(a), (0, 0, 0) site is occupied by Pu, while (0.25, 0.25, 0.25) and (0.75, 0.75, 0.75) sites are occupied by H. The space group of fcc PuH_3 is also $Fm3m$ as seen in Fig. 1(b), even though it is formed when extra H atoms enter into the octahedral interstices. Unlike PuH_2, its H atomic positions are (0.25, 0.25, 0.25) and (0.5, 0.5, 0.5), and the $1\times1\times1$ supercell of fcc PuH_3 is used in all our calculations. There are 4 Pu atoms and 12 H atoms in the supercell.

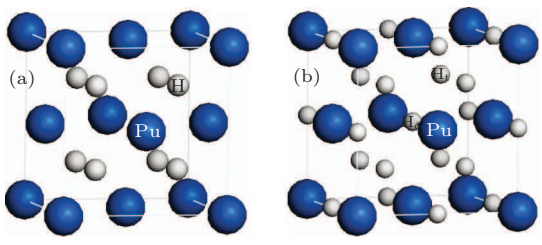


Fig. 1. (color online) Crystal structures of (a) fcc PuH_2 and (b) fcc PuH_3.

The Murnaghan equation of states are used for the determination of the static equilibrium properties.[20] The optimized results of PuH_2 and PuH_3 are shown in Tables 1 and 2, respectively.

3. Results and discussion

3.1. Structural properties

From Table 1 for PuH_2, we can see that both LSDA and GGA severely underestimate the lattice parameter with respect to the experimental value. A similar case happens for PuH_3 as shown in Table 2. After turning on Hubbard parameter U with the SO, the lattice constants of both PuH_2 and PuH_3 are much closer to the experimental values in contrast with those obtained in pure DFT and DFT+U. For PuH_2, the discrepancy between the experiment and our calculation decreases from 5.7% for GGA to 0.44% for GGA + sp + U + SO; even GGA + sp and GGA + sp + U are better than GGA. For PuH_3, it is in good agreement with the experimental value. The difference decreases from 5.43% for GGA to 0.06% (0.21%) for GGA + sp + U + SO in the FM (AFM) states, and even the results from other formalisms are in reasonable agreement with the experimental value. Some theoretical values calculated in other methods, LMTO, RLMTO, and spin-polarized LMTO, for the lattice parameter of PuH_2 are also shown in Table 1. We find that our results are much better than the others, suggesting the advantage of the present method (GGA + sp + U + SO) over the others for treating the Pu–H system in the aspect of structure.

Table 1. Structural properties of PuH_2: lattice constant a_0 and bulk modulus B_0 optimized with GGA (sp/sp + U/sp + U + SO) and LSDA (sp/sp + U/sp + U + SO). The Hubbard parameter U is 0.29 Ry.

Method	a_0/Å	B_0/GPa
GGA	5.089	83.17
LSDA	4.947	97.58
GGA + sp	5.365	60.44
GGA + sp + U	5.463	56.82
GGA + sp + U + SO	5.371	59.64
LSDA + sp	5.184	72.24
LSDA + sp + U	5.288	70.99
LSDA + sp + U + SO	5.202	71.10
LMTO[a)]	4.74	–
RLMTO[a)]	4.89	–
Spin-polarized LMTO[a)]	4.98	–
Exp.[b)]	5.395±0.002	–

[a)]Ref. [21]; [b)]Refs. [22] and [23].

The lattice parameter is changed when U or SO is included. It is clear that the lattice parameter increases as soon as the electron correlation is carefully included, which can be explained as follows. When Hubbard U is introduced, the localization of the 5f electrons of Pu will be enhanced, while the cohesion of the crystal is further decreased, which results in the increase of the lattice constant. Notice that the result from GGA + sp + U of PuH_2 is $a_0 = 5.463$ Å, which overestimates the value by 1.3%. Besides, the lattice parameters from LSDA/+ sp/+ sp + U for both PuH_2 and PuH_3 are smaller than

the corresponding values of GGA/+ sp/+ sp + U. This is because the cohesion of the crystal is greatly overestimated in the LSDA/+ sp/+ sp + U frameworks. Moreover, the lattice parameter is reduced slightly in the GGA + sp + U+ SO framework compared with that in the GGA + sp + U scheme, which is also consistent with other experimental measurements.[1,24]

Table 2. Structural properties of PuH_3 : lattice constant a_0 and bulk modulus B_0 optimized with GGA (sp/sp + U/sp + U + SO) and LSDA (sp/sp + U/sp +U + SO). The Hubbard parameter U is 0.29 Ry.

Phase	Method	a_0/Å	B_0/GPa
Nonmagnetic	GGA	5.056	116.47
	LSDA	4.939	133.48
Ferromagnetic	GGA + sp	5.252	94.19
	GGA + sp + U	5.344	82.99
	GGA + sp + U + SO	5.343	87.96
	LSDA + sp	5.118	113.97
	LSDA + sp + U	5.212	99.76
	LSDA + sp + U + SO	5.250	102.95
Antiferromagnetic	GGA + sp	5.262	92.13
	GGA + sp + U	5.352	83.04
	GGA + sp + U + SO	5.351	84.89
	LSDA + sp	5.129	108.31
	LSDA + sp + U	5.222	99.81
	LSDA + sp + U + SO	5.226	101.38
–	Exp.[b)]	5.34±0.01	–

[b)]Refs. [22] and [23].

For bulk modulus B_0, the result from GGA (+ sp/+ sp + U/ + sp + U + SO) schemes is much lower than that given by LSDA (+ sp/ + sp + U/ + sp + U+ SO) formalisms for both PuH_2 and PuH_3. This also results from the binding overestimated characteristic of LSDA calculations, which is similar to the case in the study of the PuO_2 system.[1,10]

Furthermore, B_0 from the standard DFT decreases when U is added, while it increases within DFT + U + SO for both systems. In addition, the bulk modulus tends to decrease compared with that in the pure DFT when the electron correlation in the 5f shell and the SO are taken into account. Here it is indicated that the pure DFT overestimates bulk modulus B_0 in comparison with the experimental data and the DFT + U + SO results (the experimental values of B_0 are not available yet). A similar situation is found in the studies of δ-Pu,[24] rare-earth dioxides CeO_2, PrO_2, and TbO_2,[25] and the work of Söderlind *et al*.[26] also suggested the same trends.

Above all, we note that the structural properties are not reproduced well in all the LSDA methods for PuH_2 and PuH_3, so we use the GGA methods to investigate magnetic, electronic, and elastic properties in the following sections.

3.2. Magnetic properties

The total energy and the total magnetic moment for the states of non-magnetic (NM), ferromagnetic (FM), and antiferromagnetic (AFM) phases calculated for PuH_2 and PuH_3 are shown in Table 3.

Table 3. Compilation of data on NM, FM, and AFM states of fcc PuH_2 and fcc PuH_3: total magnetic moment μ_{tot} for the supercell, total energy E_0, $\Delta E = E_{FM} - E_{AFM}$. The Hubbard parameter U is 0.29 Ry.

Compound	Method	Phase	μ_{tot}/μ_B	E_0/Ry	ΔE/Ry
PuH_2	GGA	NM	–	-59386.2967	–
	GGA + sp	FM	22.76102	–59386.4822	0.0001
		AFM	–0.00223	–59386.4823	
	GGA + sp + U	FM	21.56283	–59386.8211	–0.0268
		AFM	0.00337	–59386.7943	
	GGA + sp + U + SO	FM	21.02232	–59387.3397	–0.0002
		AFM	–0.00046	–59387.3395	
PuH_3	GGA	NM	–	–59387.5880	-
	GGA + sp	FM	20.07218	–59387.6711	–0.0025
		AFM	0.01036	–59387.6686	
	GGA + sp + U	FM	20.19049	–59387.9724	0.0002
		AFM	–0.00360	–59387.9726	
	GGA + sp + U + SO	FM	19.77723	–59388.5243	–0.0020
		AFM	–0.00001	–59388.5223	

We find that the total energy of the NM phase is the highest in the GGA scheme, in other words, the NM phase is unstable for PuH_2 and PuH_3.

For PuH_2, the results from GGA + sp + U and GGA + sp + U + SO indicate that the fcc PuH_2 is FM, and the energy differences between the FM and the AFM states are 0.0268 Ry and 0.0002 Ry, respectively. The results from GGA + sp illustrate that the fcc PuH_2 is AFM. However, it should be noted here that the energy difference between the FM and the AFM states is 0.0001 Ry within the GGA + sp scheme, and it is so small that the AFM phase is unstable. Thus, it reveals that the fcc PuH_2 is FM, which is consistent with the available experimental results.[15]

For PuH_3, the results from GGA + sp and GGA + sp + U + SO indicate that the fcc PuH_3 is FM, and the energy differences between the FM and the AFM states are 0.0025 Ry and 0.002 Ry, respectively. Meanwhile, the results from the GGA + sp + U framework illustrate that the fcc PuH_3 is AFM. How-

ever, it is important to note that the energy difference between the FM and the AFM states is 0.0002 Ry within the GGA + sp + U scheme, and it is so small that the AFM phase is unstable. Hence, the results indicate that the fcc PuH_3 is FM.

In the following sections, the calculations are performed based on the results that fcc PuH_2 and fcc PuH_3 are FM.

3.3. Electronic properties

The density of states (DOS) of fcc PuH_2 is shown in Fig. 2. The total DOS curves in four cases (GGA, GGA + sp, GGA + sp + U, GGA + sp + U + SO) all cross over the Fermi level (E_F) with a nonzero occupation of Pu 5f electrons on it. The total DOS of PuH_2 is almost composed of that of Pu atoms, moreover, the DOS of Pu atoms is dominated by the 5f partial DOS. However, there is a gradual reduction in the density of states at the Fermi level when sp, U, and SO are added one by one. When the Coulomb interaction is considered, prominent changes happen in the DOS of the GGA + sp + U calculation. The three main peaks of 5f partial DOS are much sharper and further separated than those of GGA + sp, which indicates that the localization of 5f electrons is highly strengthened in the GGA + sp + U calculation. In addition, the total DOS moves to a lower energy level when the SO is added. But, above all, the material still exhibits the metallic ground state in agreement with our previous work[3] taking into account the SO.

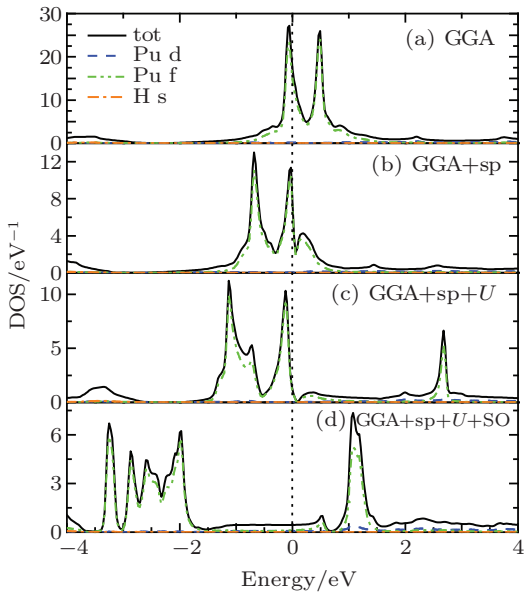


Fig. 2. (color online) Densities of states in (a) GGA, (b) GGA + sp, (c) GGA + sp + U, and (d) GGA + sp + U + SO for fcc PuH_2. The Fermi level is at 0 eV.

In order to analyze the Pu–H interaction, the PDOS for Pu d and H s orbitals are plotted in Fig. 3. In the lower part of the valence bands, from −1.5 eV to −7.0 eV, the DOS of Pu d and H s have sharp peaks at the equivalent energy, the hybridization to some extent exists between Pu d and H s occupied states. The interesting hybridization effect implies certain covalent character in the bonding of the PuH_2 system.

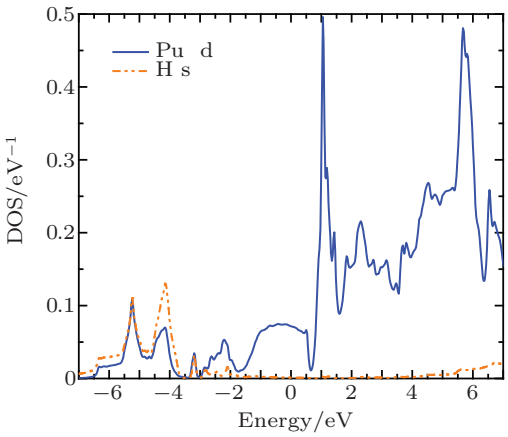


Fig. 3. (color online) Partial densities of states for the Pu d and H s of PuH_2.

For PuH_3, the densities of states in GGA + sp/ + sp + U/ + sp + SO/sp + U+ SO schemes are plotted in Fig. 4. It is clear that there is a nonzero occupation of Pu 5f states at the Fermi level in all these frames except for GGA + sp + U + SO, hence the standard DFT even DFT + U or DFT + SO predicts a metallic ground state for PuH_3. However, the GGA + sp + U + SO method not only is good at reproducing the lattice constant but also predicts a semi-conductive state. Hence, the spin–orbit coupling with Hubbard U finally leads to the semi-conducting state.

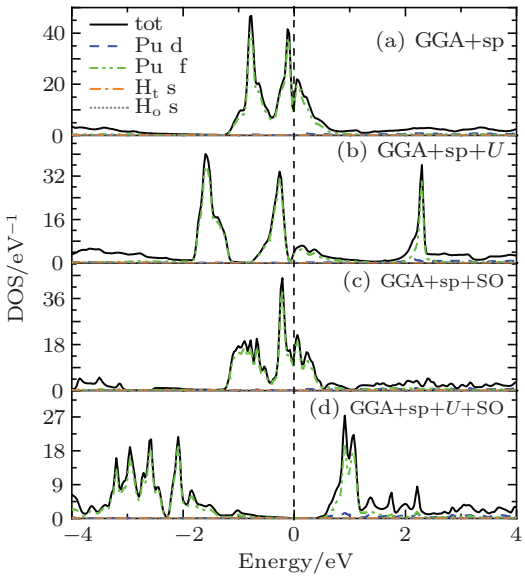


Fig. 4. (color online) The DOS in (a) GGA + sp, (b) GGA + sp + U, (c) GGA + sp + SO, and (d) GGA + sp + U + SO for fcc PuH_3. The Fermi level is at 0 eV.

The PDOS in the GGA + sp + U + SO scheme are plotted in Fig. 5 to investigate the contributions of each angular momentum for PuH_3. Obviously, the total DOS is constituted by that of Pu atoms, moreover the DOS of Pu atoms is made up

with Pu f electrons. Unlike Pu f, the Pu d orbits contribute a little to the total DOS, as well as the states of H_t s and H_o s.

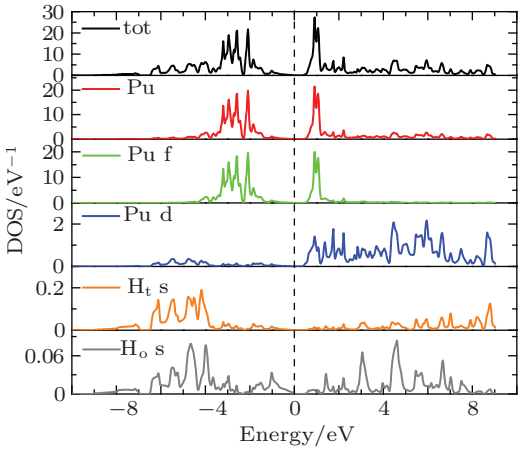


Fig. 5. (color online) The PDOS in GGA + sp + U + SO for fcc PuH_3. The Fermi level is at 0 eV.

The PDOS for Pu d, H_t s, and H_o s are plotted in Fig. 6. Hybridizations exist between Pu d and H s orbitals. In particular, Pu d and the H_t hybridize pronouncedly, which illuminates that the bonding between them has certain covalent character. However, the hybridization between Pu d and the H_o s is much weaker, namely, there is little covalent character in the bonds. This can be confirmed by the later charge density analysis.

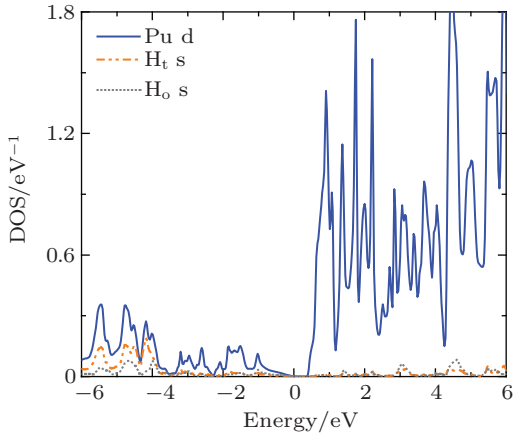


Fig. 6. (color online) The PDOS for the Pu d, H_t s, and H_o s of PuH_3.

The interpretation on the chemical bonding is further substantiated by the analysis of the valence-electron charge density and the difference charge densities along the (1 1 0) plane of the crystal structure for fcc PuH_2 and fcc PuH_3, and the charge distributions are shown in Figs. 7 and 8.

In Fig. 7(a), the valence charge density is increased gradually when approaching Pu atomic nuclei. It reflects that most of the electrons are bound around the atomic nuclei, only a few valence electrons can escape the bondage of the nuclei. It can be clearly seen that appreciable charge exists in the outer regions of Pu and H atoms, and much charge of Pu atoms is lost to the interstitial regions.[27] It is proved by the difference electron charge density in Fig. 7(b). In particular, it is important to note that the charge, to some extent, piles up in the bonding regions between different atoms. This feature reflects that the bonding of Pu and H atoms has certain covalent character in the PuH_2 system. However, there is much light charge buildup with the typical characteristic of metallic bonding in the interstices regions away from the bonds, which suggests that PuH_2 is metallic as indicated by the DOS analysis.

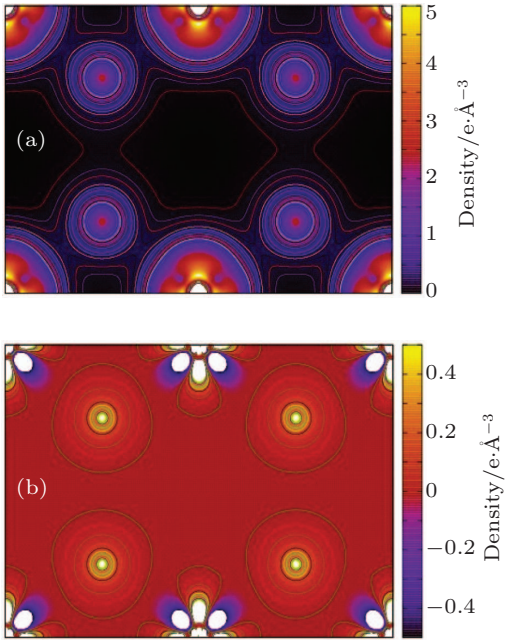


Fig. 7. (color online) Calculated (a) valence-electron-charge and (b) difference electron-charge density contour plots from the GGA + sp + U + SO calculation for fcc PuH_2 in the (1 1 0) plane.

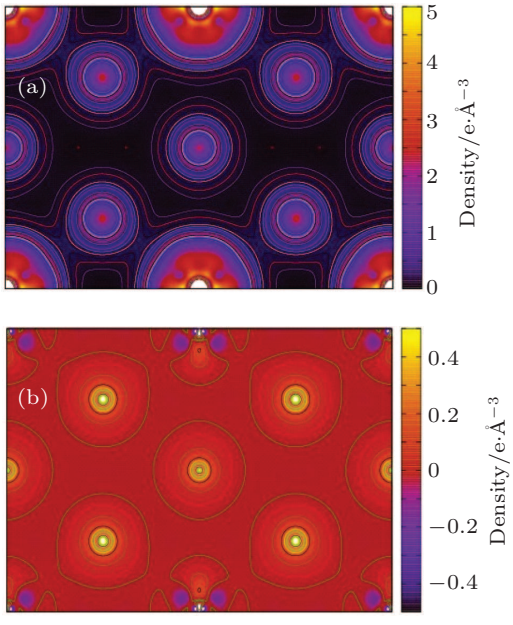


Fig. 8. (color online) Calculated (a) valence-electron-charge density and (b) difference electron-charge contour plots from the GGA + sp + U + SO calculations for fcc PuH_3 in the (1 1 0) plane.

For PuH_3 in Fig. 8(a), it is clear that almost no charge accumulates in the bonding regions between Pu and H_o atoms while appreciable charge distributes in the bonding regions between Pu and H_t atoms, which strengthens the judgments of certain covalent character of PuH_3. However, no localized, covalent bond charge can be detected, suggesting that the local Pu–H_o interactions are ionic. In addition, the difference electron-charge density contour plot reveals that most charge of Pu atoms moves to H_t atoms except for a little to H_o atoms, as shown in Fig. 8(b). So, we believe that the bonding of Pu and H_o atoms has a relatively strong ionic character.

3.4. Elastic properties

In this study, we compute the elastic constants c_{ij} in GGA + sp, GGA + sp + U, and GGA + sp + U + SO respectively. Fcc PuH_2 and fcc PuH_3 have only three elastic constants, c_{11}, c_{12}, and c_{44} owing to the cubic symmetry. The elastic constants and the mechanical properties derived from these states are shown in Tables 4 and 5. The bulk modulus B, Young modulus Y, and Poisson's ratio are obtained by the Voigt formalism: $B = (c_{11} + 2c_{12})/3$, $Y = 9BG/(G + 3B)$, and $\sigma = (B - 2G/3)/(2B + 2G/3)$, where G is the shear modulus defined by $G = (c_{11} - c_{12} + 3c_{44})/5$. The necessary conditions for mechanical stability are given by $(c_{11} - c_{12}) > 0$, $(c_{11} + 2c_{12}) > 0$, $c_{11} > 0$, $c_{44} > 0$ for cubic crystal structures.

One can notice that c_{11}, c_{12}, and c_{44} for fcc PuH_2 and fcc PuH_3 satisfy the necessary conditions of mechanical stability. For PuH_2, c_{11}, c_{12}, and c_{44} from the GGA + sp + U + SO frame are almost the largest except c_{12}, meanwhile bulk modulus B, shear modulus G, and Young modulus Y show the same tendency that the values from the GGA + sp + U + SO frame are almost the largest. Bulk modulus B obtained from the GGA + sp + U + SO frame agrees well with that from the Birch–Murnaghan equation of state.

The bulk modulus is a fundamental physical quantity of solids and can be used as a measure of the average bond strengths of atoms of crystals. Furthermore, shear modulus G and Young modulus Y can illustrate the stability of material. The results in Tables 4 and 5 indicate that the state of PuH_3 is more stable than that of PuH_2 in the GGA + sp + U + SO frame. Generally, the elastic constants of metals are smaller than those of semiconductors. Our result also follows the tendency since PuH_2 (PuH_3) is metallic (semiconductor) in the GGA + sp + U + SO scheme. To the best of our knowledge, the elastic constants have not yet been measured experimentally and calculated theoretically for both PuH_2 and PuH_3, so there are currently no experimental or theoretical data for this elastic modulus to be compared with. Hence our results can help to design future experiments to investigate the stability of PuH_2 and PuH_3.

Table 4. Elastic constants c_{11}, c_{12}, c_{44}, bulk modulus B, shear modulus G, Young modulus Y, and Poisson's ratio σ for PuH_2 in GGA methods.

Method	c_{11}/GPa	c_{12}/GPa	c_{44}/GPa	B/GPa	Y/GPa	G/GPa	σ
sp	70.44	47.07	65.02	54.86	103.57	43.69	0.185
sp + U	71.10	34.37	26.44	46.61	59.72	23.21	0.287
sp + U + SO	130.51	45.65	77.06	73.94	147.57	63.21	0.167

Table 5. Elastic constants c_{11}, c_{12}, c_{44}, bulk modulus B, shear modulus G, Young modulus Y, and Poisson's ratio σ for PuH_3 in GGA methods.

Method	c_{11}/GPa	c_{12}/GPa	c_{44}/GPa	B/GPa	Y/GPa	G/GPa	σ
sp	130.29	67.65	101.21	88.53	172.25	73.25	0.310
sp + U	138.85	58.81	121.41	85.49	197.97	88.85	0.114
sp + U + SO	140.77	75.46	133.16	97.23	211.48	92.96	0.137

4. Conclusion

We have performed a detailed investigation on the structural, magnetic, electronic, and elastic properties of fcc PuH_2 and fcc PuH_3 within the DFT framework by using the FP-LAPW technique. Our results indicate that fcc PuH_2 is metallic and fcc PuH_3 is a semiconductor with an energy gap of about 0.35 eV. The latter is more stable in ferromagnetic phases even the energy difference of the ground state between ferromagnetic and antiferromagnetic states is small. The bonds for PuH_2 have mainly covalent character while there are covalent bonds in addition to apparent ionicity bonds for PuH_3. The mechanical stability of fcc PuH_2 and fcc PuH_3 is investigated with elastic constant calculation, which also employs the GGA + sp + U + SO frame. Moreover, we find that the GGA + sp + U + SO calculation predicts very well not only the lattice constant but also the observed energy gap which cannot emerge within other schemes such as DFT or even DFT + U. This fact emphasizes the important role of both the strong correlation effects and the SO in calculating the electronic states. It is also predicted that the metal–insulator transition takes place from fcc PuH_2 to fcc PuH_3 for the first time.

Acknowledgement

We are grateful to Peng Li, Lei Wan, and Peng Shi for helpful comments and discussion.

References

[1] Moore K T and van der Laan G 2009 *Rew. Mod. Phys.* **81** 235
[2] Ao B Y, Ai J J, Gao T, Wang X L, Shi P, Chen P H and Ye X Q 2012 *Chin. Phys. Lett.* **29** 017102
[3] Ai J J, Liu T, Gao T and Ao B Y 2012 *Comput. Mater. Sci.* **51** 127
[4] Ao B Y, Wang X L, Shi P, Chen P H, Ye X Q, Lai X C and Gao T 2012 *J. Nucl. Mater.* **424** 183
[5] Ao B Y, Wang X L, Shi P, Chen P H, Ye X Q, Lai X C, Ai J J and Gao T 2012 *Int. J. Hydrogen Energ.* **37** 5108
[6] Ao B Y, Xia J X, Chen P H, Hu W Y and Wang X L 2012 *Chin. Phys. B* **21** 026103
[7] Hecker S S 2008 *Metall. Mater. Trans. A* **39A** 1585
[8] Murtaza G, Amin B, Arif S, Maqbool M, Ahmad I, Afaq A, Nazir S, Imran M and Haneef M 2012 *Comput. Mater. Sci.* **58** 71
[9] Shim J H, Haule K and Kotliar G 2007 *Nature* **446** 513
[10] Sun B, Zhang P and Zhao X G 2008 *J. Chem. Phys.* **128** 084705
[11] Liu T, Cai T, Gao T and Li G 2010 *Physica B* **405** 3717
[12] Wang B T and Zhang P 2011 *Chin. Phys. Lett.* **28** 047101
[13] Wang H and Konashi K 2012 *J. Alloys Compd.* **533** 53
[14] Nakamura H, Machida M and Kato M 2010 *Phys. Rev. B* **82** 155131
[15] Aldred A T, Cinader G, Lam D J and Weber L W 1979 *Phys. Rev. B* **19** 300
[16] Willis J O, Ward J W, Smith J L, Kosiewicz S T, Haschke J M and Hodges III A E 1985 *Physica B* **130** 527
[17] Blaha P, Schwarz K, Madsen G K H, Kvasnicka D and Luitz J 2011 *WIEN2k an Augmented Plane Wave + Local Orbitals Program for Calculating Crystal Properties* (Austria: Karlheinz Schwarz Technische Universität Wien)
[18] Singh D J 1994 *Planewaves, Pseudopotentials and the LAPW Method* (Boston: Kluwer Academic)
[19] Kuneš J, Novak P, Diviš M and Oppeneer P M 2001 *Phys. Rev. B* **63** 205111
[20] Murnaghan F D 1944 *Proc. Natl. Acad. Sci. USA* **30** 244
[21] Brooks M M S and Johansson B 1985 *Physica B+C* **130** 516
[22] Mulford R N R and Sturdy G E 1955 *J. Am. Chem. Soc.* **77** 3449
[23] Mulford R N R and Sturdy G E 1956 *J. Am. Chem. Soc.* **78** 3897
[24] Kanoun M B, Reshak A H, Bouayed K N and Said G S 2012 *J. Magn. Magn. Mater.* **324** 1397
[25] Bouchet J, Siberchicot B, Jollet F and Pasturel A 2000 *J. Phys.: Condens. Matter* **12** 1723
[26] Söderlind P, Eriksson O, Johansson B and Wills J M 1994 *Phys. Rev. B* **50** 7291
[27] Eriksson O, Hao Y G, Cooper B R, Fernando G W, Cox L E, Ward J W and Boring A M 1991 *Phys. Rev. B* **43** 4590